

UC Santa Cruz

UC Santa Cruz Previously Published Works

Title

The NMR-Rosetta capsid model of M13 bacteriophage reveals a quadrupled hydrophobic packing epitope

Permalink

<https://escholarship.org/uc/item/2790w0fg>

Journal

Proceedings of the National Academy of Sciences of the United States of America, 112(4)

ISSN

0027-8424

Authors

Morag, Omry
Sgourakis, Nikolaos G
Baker, David
et al.

Publication Date

2015-01-27

DOI

10.1073/pnas.1415393112

Peer reviewed

The NMR–Rosetta capsid model of M13 bacteriophage reveals a quadrupled hydrophobic packing epitope

Omry Morag^a, Nikolaos G. Sgourakis^{b,1}, David Baker^b, and Amir Goldbourt^{a,2}

^aSchool of Chemistry, Raymond and Beverly Sackler Faculty of Exact Sciences, Tel Aviv University, Ramat Aviv 69978, Tel Aviv, Israel; and ^bDepartment of Biochemistry, University of Washington, Seattle, WA 98195

Edited by Michael G. Rossmann, Purdue University, West Lafayette, IN, and approved December 23, 2014 (received for review August 12, 2014)

Filamentous phage are elongated semiflexible ssDNA viruses that infect bacteria. The M13 phage, belonging to the family Inoviridae, has a length of ~1 μm and a diameter of ~7 nm. Here we present a structural model for the capsid of intact M13 bacteriophage using Rosetta model building guided by structure restraints obtained from magic-angle spinning solid-state NMR experimental data. The C5 subunit symmetry observed in fiber diffraction studies was enforced during model building. The structure consists of stacked pentamers with largely alpha helical subunits containing an N-terminal type II β-turn; there is a rise of 16.6–16.7 Å and a tilt of 36.1–36.6° between consecutive pentamers. The packing of the subunits is stabilized by a repeating hydrophobic stacking pocket; each subunit participates in four pockets by contributing different hydrophobic residues, which are spread along the subunit sequence. Our study provides, to our knowledge, the first magic-angle spinning NMR structure of an intact filamentous virus capsid and further demonstrates the strength of this technique as a method of choice to study noncrystalline, high-molecular-weight molecular assemblies.

solid-state NMR | magic-angle spinning | filamentous bacteriophage | structure determination | Rosetta modeling

Filamentous bacteriophage are long, thin, and semiflexible rod viruses that infect bacteria (1, 2). These large assemblies (~15–35 MDa) contain a circular single-stranded (ss) DNA genome encapsulated in a protein shell. All filamentous phage have a similar life cycle and virion structure despite the relatively high number of strains, with DNA sequence homology varying from almost complete to very little. The unique phage properties make them ideal for a large range of applications such as phage display (3), DNA cloning and sequencing (4, 5), nanomaterial fabrication (6–8), and as drug-carrying nanomachines (9). In addition, filamentous viruses form a variety of liquid crystals driving the development of both theory and practice of soft-matter physics (10, 11). Filamentous viruses are also associated with various diseases, e.g., CTXφ phage in cholera toxin (12) and Pf4 phage in cystic fibrosis (13).

Phage belonging to the Ff family (M13, fd, f1) are F-pilus-specific viruses that share almost identical genomes and very similar structures. M13 is a 16-MDa virus having a diameter of ~7 nm and a length of ~1 μm. The capsid is composed of several thousand identical copies of a major coat protein subunit arranged in a helical array surrounding a core of a circular ssDNA. The major coat proteins constitute ~85% of the total virion mass, the ssDNA ~12%, and all other minor proteins (gp3, gp6, gp7, gp9) that are specific for infection and assembly constitute about 3% of the total virion mass (1, 14).

Previous structural models for a small number of phages have been obtained by means of X-ray fiber diffraction (15–19), static solid-state NMR (20, 21), and cryo-EM (22). Structural models for the Ff family have been proposed based on the three methods; however, satisfactory resolution was only obtained for the Y21M mutant of the fd phage (17, 18, 21) (*wt* fd is related to M13 by one additional mutation, N12D). The only reported model for M13 (23) (no coordinates available) and models of

fd-Y21M from different methods differ in detail (24) and lack accuracy in some structural details such as the N-terminus orientation, the nature of DNA–protein interactions, and sidechain interactions, which are the dominant packing elements of the capsid. The most recent model was built using a combination of static NMR and fiber diffraction (17).

According to fiber diffraction, the symmetry of the Ff capsid is C₅S₂, also referred to as class I symmetry. That is, a fivefold rotation of the major coat protein subunit around the virion axis (pentamers) and an approximate 36° rotation relating two successive pentamers [in fd-Y21M a precise 36° rotation was reported; for fd, values of –33.23° (18) and –34.62° (22) were reported]. All studies report that the coat protein is mostly right-handed, curved, α-helical, with a flexible or disordered N terminus.

Magic-angle spinning (MAS) solid-state NMR has become a popular tool for studying the structure and dynamics of biological molecules (25–27). The method can be implemented on a variety of systems from small peptides to macromolecular biological assemblies. Integrated approaches can be used to resolve structures of large assemblies (28, 29) and recently, the combination of MAS NMR data, cryo-EM, and Rosetta modeling resulted in a detailed atomic structure of the recombinant type III secretion system needle (30, 31). We have previously performed MAS NMR studies on both *wt* fd and M13 in a precipitated form (32–34). Their chemical shifts pointed to a single

Significance

We present an atomic-resolution structure of the M13 filamentous bacteriophage capsid, one of many filamentous viruses that play important roles in many areas of research. The model was obtained by combining magic-angle spinning NMR and Rosetta modeling, used for the first time, to our knowledge, to derive the atomic structure of an intact virus capsid. The structure is made up of thousands of identical helical subunits stabilized by repeating hydrophobic pockets, which serve as a locking motif, suggesting a direct role in phage particle assembly. Analysis of various phage sequences suggests the presence of a conserved design principle for helical capsids. Because the current method does not rely on any particular preparation procedure, it can be applied to other viral capsids and molecular assemblies.

Author contributions: A.G. designed research; O.M. and N.G.S. performed research; D.B. contributed new reagents/analytic tools; O.M. and N.G.S. analyzed data; O.M. prepared phage samples and performed NMR experiments; N.G.S. and D.B. designed and performed calculations; and O.M., N.G.S., and A.G. wrote the paper.

The authors declare no conflict of interest.

This article is a PNAS Direct Submission.

Data deposition: The atomic coordinates, NMR chemical shifts, and restraints have been deposited in the Protein Data Bank, www.pdb.org (PDB ID code 2MJZ), and Biological Magnetic Resonance Bank, www.bmr.bwisc.edu/ (accession no. 19747).

¹Present address: Laboratory of Chemical Physics, National Institute of Diabetes and Digestive and Kidney Diseases, National Institutes of Health, Bethesda, MD 20892.

²To whom correspondence should be addressed. Email: amirgo@post.tau.ac.il.

This article contains supporting information online at www.pnas.org/lookup/suppl/doi:10.1073/pnas.1415393112/-DCSupplemental.

homogeneous capsid subunit that is mostly helical and curved with a mobile N terminus. NMR studies of the interactions between the capsid and the DNA reported on the subunit orientation with respect to the viral axis, and indicated that the C terminus undergoes electrostatic interactions with the DNA.

In this study, we use homonuclear 2D ^{13}C - ^{13}C correlation experiments on sparsely labeled M13 samples together with our prior backbone and sidechain resonance assignments of the M13 phage to acquire MAS NMR structure restraints. Using the CS-Rosetta fold-and-dock protocol (35) we derive an atomic detailed well-converged quaternary structural model of the intact M13 phage viral capsid. The specific bacteriophage symmetry produces four identical, repeating hydrophobic pockets for each subunit, resulting in tight subunit packing that stabilizes the phage assembly.

Results

Acquisition of MAS NMR Distance Restraints. Chemical shifts of the M13 capsid were obtained previously (33) and deposited in the Biological Magnetic Resonance Bank (accession no. 19747). Both intra- and intersubunit distance restraints used in the current study were based on the observation of cross-peaks in 2D ^{13}C - ^{13}C correlation experiments reporting on through-space proximities between carbon atoms. In uniformly labeled samples, peak linewidths resulting from scalar couplings can be narrowed by the application of selective pulses (36). Here enhanced resolution was obtained by virtue of the “checkerboard” labeling pattern stemming from the metabolism of glycerol in *Escherichia coli* (37); sparsely labeled M13 samples were prepared by infecting cells in a minimal medium containing either $[1,3-^{13}\text{C}]$ -glycerol (1,3-gly-M13) or $[2-^{13}\text{C}]$ -glycerol (2-gly-M13). Both samples exhibited improved dispersion due to the elimination of many unlabeled carbon peaks.

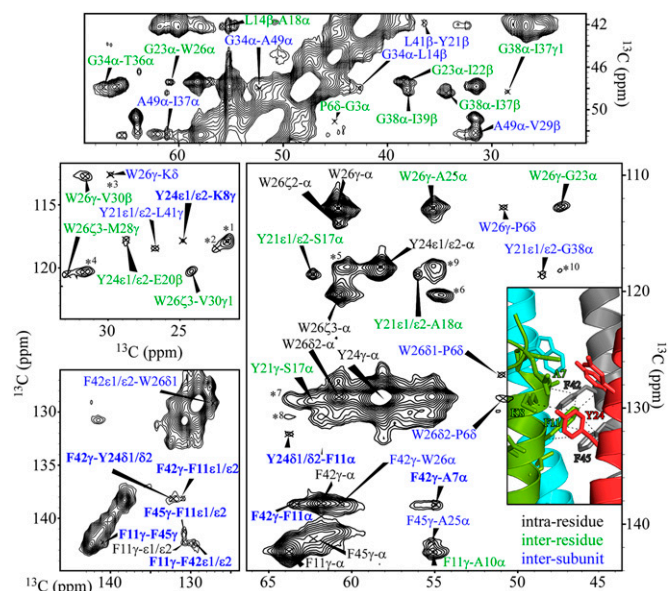


Fig. 2. A spectrum of 2-gly-M13 obtained from CORD500 experiment. The contact pocket includes subunits P_{45} (green), P_{55} (red), P_{64} (cyan), and P_{74} (gray). The spectrum was apodized with a 100-Hz exponential function in both dimensions and drawn as in Fig. 1. A more complete assignment of all signals in the top spectrum appears in *SI Appendix, Fig. S3*. A list of the ambiguous signals appears in *SI Appendix, Table S1*.

Excerpts from data sets acquired using both samples are shown in Figs. 1 and 2, respectively. Cross-peaks corresponding to sequential, helical (interresidue contacts between residues i, j such that $2 \leq |i - j| \leq 4$), and long-range contacts ($|i - j| > 4$) are highlighted. Due to the helical nature of the subunit, those long-range contacts correspond to proximities between different subunits and are therefore referred to as intersubunit contacts. In the two spectra these contacts are indicated in the cartoon view of the final capsid assembly. Here we chose a particular subunit and show its interactions with neighboring subunits. The actual assignment of such contacts to a particular subunit number was only obtained after the completion of structure calculation, as discussed in *Determination of the Structure of the M13 Bacteriophage Capsid*.

The notation we use for describing the capsid arrangement is based on the pentamer symmetry; each subunit P_{nm} is given two indices, where the index n indicates the pentamer number (n between 1 and 7, where $n = 1$ corresponds to the C-terminal part) and m indicates the identity of the subunit within each pentamer ($m = 1-5$). In Fig. 1, subunit P_{45} in green, for which contacts are shown, corresponds to pentamer number 4—subunit number 5 in the 35-subunit assembly. Also shown are P_{55} in red and P_{35} in cyan. In Fig. 2, the four subunits are P_{45} in green, P_{55} in red, P_{64} in cyan, and P_{74} in gray.

The N-terminal part of M13 is not part of the subunit helix and shows residual conformational flexibility (33, 38). The N-terminus connectivities shown in Fig. 3, observed in our homonuclear correlation spectra (D5–W26 in Fig. 1 and E2–E20 in *SI Appendix, Fig. S1*), demonstrate that restraints acquired on this part are sufficient to define its position and conformation as well. Such data were previously inconclusive or inaccessible by other methods.

In total, 95 nonambiguous intersubunit restraints and 160 intrasubunit restraints were collected from all our spectra and used during Rosetta modeling. Distance restraints were between 1.5 Å and either 5, 7, or 8.2 Å. The 5-Å limit was imposed using the tryptophan residue as a standard by correlating possible

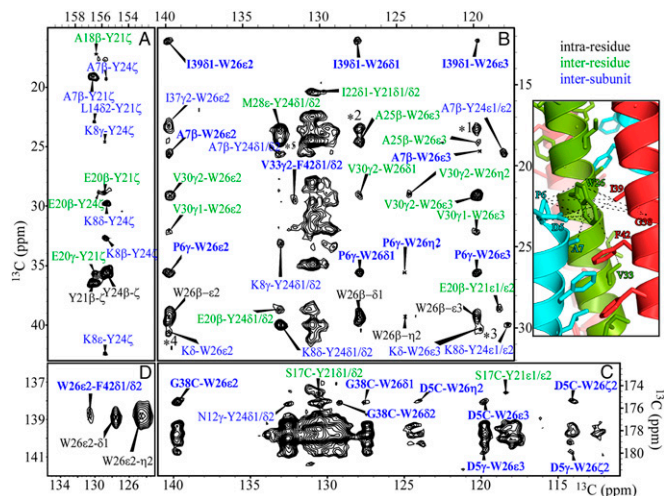


Fig. 1. Two-dimensional ^{13}C - ^{13}C CORD MAS NMR spectrum of intact 1,3-gly-M13 obtained using a mixing time of 500 ms (CORD500). The spectrum shows intrasubunit contacts (black), interresidue contacts within the same subunit (green), and intersubunit contacts (blue). (Inset, Right) contact pocket between the three subunits P_{45} (i.e., pentamer number 4—subunit number 5) in green, P_{55} in red, and P_{35} in cyan. The dashed lines correspond to the highlighted (bold) intersubunit cross-peaks shown in the spectrum. Spectra A, B, and C were generated by apodizing the data with a Lorentz-to-Gauss transformation in both dimensions and are drawn using 15 contour levels (multiplicity of 1.2) starting at 5 times the noise root-mean-square. Spectrum D was apodized with a 100-Hz exponential function and drawn at similar contour levels. Peaks with ambiguity are marked by *# if they have only few options and are tabulated in *SI Appendix, Table S1*. Signals in the region of 130 ppm and several carbonyl signals are highly ambiguous and are unassigned here.

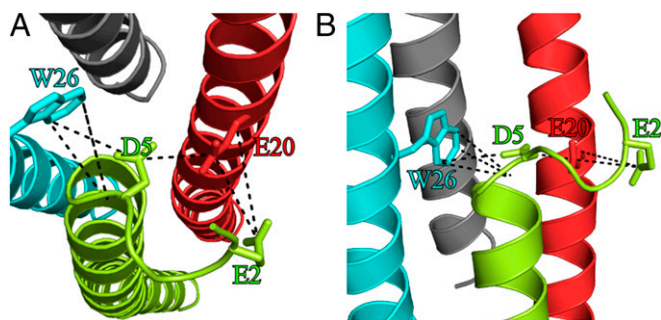


Fig. 3. NMR-based contacts in the N terminus. (A) Top view and (B) side view.

distances in the Trp sidechain to peak intensities in CORD150 (combined $R2_n^*$ -driven recoupling with a mixing time of 150 ms) and CORD500 experiments (*Materials and Methods* and *SI Appendix*, Fig. S2). A separate local field experiment (39) performed on a 2-gly-M13 sample verified that this residue is indeed rigid and can be used for this purpose. Upper distance limits for each restraint in the DARR500 (dipolar assisted rotational resonance) and CORD500 experiments were set to 7 Å. The 8.2-Å limit was used for restraints including aromatic ring carbons due to the ambiguity between atoms across the ring (e.g., TyrC δ 1–C δ 2, PheC ϵ 1–C ϵ 2). The addition of 1.2 Å defines the distance from the center of the aromatic ring to atoms at opposite positions in the ring.

Determination of the Structure of the M13 Bacteriophage Capsid. We carried out calculations using a system consisting of 35 subunits, arranged in seven pentamers, which is sufficient to describe all of the unique interactions of a “master” subunit in the entire assembly and allow for efficient Rosetta energy calculations (40). The backbone, sidechain, and rigid-body degrees of freedom (radius, rise, and rotation per pentamer along the fiber axis and relative subunit orientation) were optimized in Rosetta calculations to simultaneously minimize the system energy and maximize the fit to the NMR restraints.

Structure calculations were obtained in two steps. In the first stage, only nonambiguous restraints, collected from several DARR and CORD experiments, were considered (a total of 214 contacts; 59 intersubunit, 155 intrasubunit). Numerous intrasubunit and sequential contacts were not included in the calculation as they do not improve the local structure resolution in the Rosetta modeling, which is determined by the physically realistic all-atom energy function. These preliminary Rosetta structure calculations generated a local α -helical subunit secondary structure as a ruler that imposes an upper limit on the sequence separation for an intrasubunit interaction (four residues maximum). Based on this upper limit, in the subsequent calculations 59 residue–residue cross-peaks were allowed to be assigned to any pair of subunits, but not to a single subunit. Large-scale optimization of the energy of the system supplemented by the experimental restraints with respect to the degrees of freedom (DOF) of the system (*Materials and Methods*) yielded a cluster of preliminary models, from which the interacting sites along the different subunits could be identified.

Following this first round of calculations, the ambiguities in the restraints could be reduced because contacts between many pairs of subunits could be ruled out based on the quaternary structure of the first round models; new nonambiguous restraints were then defined when only one contact remained with a distance below 10 Å. This elimination procedure resulted in 95 intersubunit restraints (between 34 unique amino acid pairs) and 160 intrasubunit restraints. A second round of calculations was then carried out using these restraints which yielded a converged

model of the assembly. In this final model all NMR intersubunit restraints were identified and fulfilled within 0.3 Å with the exception of six minor violations (2.6% of total restraints, averaging 1.5 Å) in the three lowest-energy structures with backbone heavy-atom rmsd of 0.47 Å and all-atom rmsd of 0.61 Å. All 95 intersubunit restraints, explicitly identified from the final model, are given in *SI Appendix*, Table S2. Examination of the number of contacts per residue (*SI Appendix*, Table S2 and Fig. S4) shows that aromatic and hydrophobic residues participate in most contacts. The Rosetta structure calculation protocol is detailed in *Materials and Methods*.

Description of the M13 Structure. The NMR–Rosetta structural ensemble of the M13 phage was deposited in the Protein Data Bank (PDB ID code 2MJZ). The radius of the virus (for the three lowest energy structures, measured from center of mass of the phage to the center of mass of one subunit) is 21.9–22.6 Å. (The outer radius of the capsid measured from the nitrogen amide of A1 is 35.2 Å, in agreement with prior reports.) As shown in Fig. 4, the rise between pentamers is 16.6–16.7 Å and the tilt is 36.1–36.6°, indicating a symmetry very close to ideal C_5S_2 . This tilt angle is defined by a right-hand rotation around the viral axis, where the N-terminal part is on the top (Fig. 4); in our notation the subunit indices follow this direction.

The detailed atomic-resolution model for M13 is shown in Fig. 5 (an overlay of a single subunit from the three lowest structures is shown in Fig. 4A). Each subunit consists of a single curved, right-handed α -helix spanning residues 6–48, which is preceded by an N-terminal type II β -turn. These secondary structure elements can also be obtained based on chemical shift prediction alone (41). As discussed above, the majority of the intersubunit contacts were observed in hydrophobic regions. Of the 95 contacts pairs, 44 involved carbons of W26, 28 involved tyrosines (Y21 or Y24), and 32 involved the phenylalanine residues F11, F42, and F45. Eighty of the 95 restraints (84%) defined one major pocket that connects four different subunits. The hydrophobic pocket, illustrated in Fig. 5B and *SI Appendix*, Fig. S5, is consistent with prior studies of fd phage [fd and M13 have almost identical NMR chemical shifts (33)], which already highlighted the importance of these hydrophobic interactions and in particular, the intercalation of F11 between F42 and F45 (18, 42). These strong interactions drive the packing of subunits because the capsid symmetry dictates that this pocket repeats every \sim 10 residues along the sequence with different combinations of the four

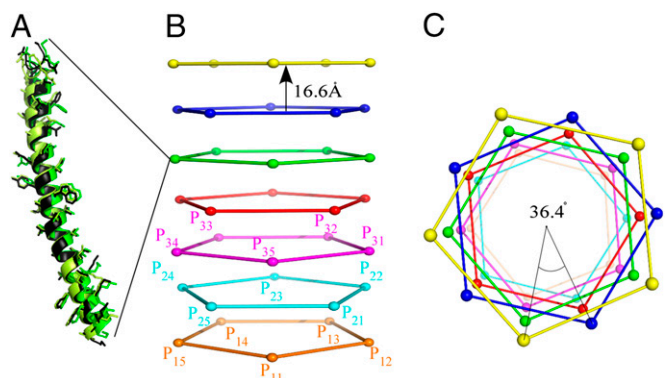


Fig. 4. Symmetry and subunit structure of M13 bacteriophage as determined from MAS ssNMR and Rosetta modeling. (A) Three subunits of the lowest-energy structures belonging to a single position (P_{52}). (B) Side view and (C) top view, showing the arrangement of 35 subunits modeled by Rosetta. Each subunit is represented by the nitrogen amide of the single proline residue in position 6. Lines between the proline amines are shown for illustrative purposes only.

- Day LA (2008) *Encyclopedia of Virology*, eds Allan G, Webster R (Elsevier, Oxford), 3rd Ed.
- Marvin DA, Symmons MF, Straus SK (2014) Structure and assembly of filamentous bacteriophages. *Prog Biophys Mol Biol* 114(2):80–122.
- Kehoe JW, Kay BK (2005) Filamentous phage display in the new millennium. *Chem Rev* 105(11):4056–4072.
- Dale RMK, McClure BA, Houchins JP (1985) A rapid single-stranded cloning strategy for producing a sequential series of overlapping clones for use in DNA sequencing: Application to sequencing the corn mitochondrial 18 S rDNA. *Plasmid* 13(1):31–40.
- Yanisch-Perron C, Vieira J, Messing J (1985) Improved M13 phage cloning vectors and host strains: Nucleotide sequences of the M13mp18 and pUC19 vectors. *Gene* 33(1):103–119.
- Hyman P (2012) Bacteriophages and nanostructured materials. *Adv Appl Microbiol* 78:55–73.
- Mao C, et al. (2004) Virus-based toolkit for the directed synthesis of magnetic and semiconducting nanowires. *Science* 303(5655):213–217.
- Lee YJ, et al. (2009) Fabricating genetically engineered high-power lithium-ion batteries using multiple virus genes. *Science* 324(5930):1051–1055.
- Clark JR, March JB (2006) Bacteriophages and biotechnology: Vaccines, gene therapy and antibacterials. *Trends Biotechnol* 24(5):212–218.
- Huang F, Rotstein R, Fraden S, Kasza KE, Flynn NT (2009) Phase behavior and rheology of attractive rod-like particles. *Soft Matter* 5(14):2766–2771.
- Barry E, Beller D, Dogic Z (2009) A model liquid crystalline system based on rodlike viruses with variable chirality and persistence length. *Soft Matter* 5(13):2563–2570.
- Waldor MK, Mekalanos JJ (1996) Lysogenic conversion by a filamentous phage encoding cholera toxin. *Science* 272(5270):1910–1914.
- Fothergill JL, et al. (2011) Effect of antibiotic treatment on bacteriophage production by a cystic fibrosis epidemic strain of *Pseudomonas aeruginosa*. *Antimicrob Agents Chemother* 55(1):426–428.
- Marvin DA (1998) Filamentous phage structure, infection and assembly. *Curr Opin Struct Biol* 8(2):150–158.
- Banner DW, Nave C, Marvin DA (1981) Structure of the protein and DNA in fd filamentous bacterial virus. *Nature* 289(5800):814–816.
- Caspar DL, Makowski L (1981) The symmetries of filamentous phage particles. *J Mol Biol* 145(3):611–617.
- Marvin DA, Welsh LC, Symmons MF, Scott WRP, Straus SK (2006) Molecular structure of fd (f1, M13) filamentous bacteriophage refined with respect to X-ray fibre diffraction and solid-state NMR data supports specific models of phage assembly at the bacterial membrane. *J Mol Biol* 355(2):294–309.
- Marvin DA, Hale RD, Nave C, Helmer-Citterich M (1994) Molecular models and structural comparisons of native and mutant class I filamentous bacteriophages Ff (fd, f1, M13), If1 and IKe. *J Mol Biol* 235(1):260–286.
- Pederson DM, et al. (2001) The protein capsid of filamentous bacteriophage PH75 from *Thermus thermophilus*. *J Mol Biol* 309(2):401–421.
- Thiriou D, Nevzorov AA, Zagyanskiy L, Wu CH, Opella SJ (2004) Structure of the coat protein in Pf1 bacteriophage determined by solid-state NMR spectroscopy. *J Mol Biol* 341(3):869–879.
- Zeri AC, Mesleh MF, Nevzorov AA, Opella SJ (2003) Structure of the coat protein in fd filamentous bacteriophage particles determined by solid-state NMR spectroscopy. *Proc Natl Acad Sci USA* 100(11):6458–6463.
- Wang YA, et al. (2006) The structure of a filamentous bacteriophage. *J Mol Biol* 361(2):209–215.
- Glucksman MJ, Bhattacharjee S, Makowski L (1992) Three-dimensional structure of a cloning vector. X-ray diffraction studies of filamentous bacteriophage M13 at 7 Å resolution. *J Mol Biol* 226(2):455–470.
- Straus SK, Scott WRP, Symmons MF, Marvin DA (2008) On the structures of filamentous bacteriophage Ff (fd, f1, M13). *Eur Biophys J* 37(4):521–527.
- Ladizhansky V (2014) Recent advances in magic-angle spinning solid-state NMR of proteins. *Isr J Chem* 54(1-2):86–103.
- Goldbourt A (2013) Biomolecular magic-angle spinning solid-state NMR: Recent methods and applications. *Curr Opin Biotechnol* 24(4):705–715.
- Tycko R (2011) Solid-state NMR studies of amyloid fibril structure. *Annu Rev Phys Chem* 62:279–299.
- Jehle S, et al. (2010) Solid-state NMR and SAXS studies provide a structural basis for the activation of alphaB-crystallin oligomers. *Nat Struct Mol Biol* 17(9):1037–1042.
- Tang M, et al. (2013) Structure of the disulfide bond generating membrane protein DsbB in the lipid bilayer. *J Mol Biol* 425(10):1670–1682.
- Loquet A, et al. (2012) Atomic model of the type III secretion system needle. *Nature* 486(7402):276–279.
- Demers J-P, et al. (2014) High-resolution structure of the *Shigella* type-III secretion needle by solid-state NMR and cryo-electron microscopy. *Nat Commun* 5:4976.
- Abramov G, Morag O, Goldbourt A (2011) Magic-angle spinning NMR of a class I filamentous bacteriophage virus. *J Phys Chem B* 115(31):9671–9680.
- Morag O, Abramov G, Goldbourt A (2011) Similarities and differences within members of the Ff family of filamentous bacteriophage viruses. *J Phys Chem B* 115(51):15370–15379.
- Morag O, Abramov G, Goldbourt A (2014) Complete chemical shift assignment of the ssDNA in the filamentous bacteriophage fd reports on its conformation and on its interface with the capsid shell. *J Am Chem Soc* 136(6):2292–2301.
- Das R, et al. (2009) Simultaneous prediction of protein folding and docking at high resolution. *Proc Natl Acad Sci USA* 106(45):18978–18983.
- Straus SK, Bremi T, Ernst RR (1998) Experiments and strategies for the assignment of fully ¹³C/¹⁵N-labelled polypeptides by solid state NMR. *J Biomol NMR* 12(1):39–50.
- LeMaster DM, Kushlan DM (1996) Dynamical mapping of *E. coli* Thioredoxin via ¹³C NMR relaxation analysis. *J Am Chem Soc* 118(9):9255–9264.
- Colnago LA, Valentine KG, Opella SJ (1987) Dynamics of fd coat protein in the bacteriophage. *Biochemistry* 26(3):847–854.
- Hong M, et al. (1997) Coupling amplification in 2D MAS NMR and its application to torsion angle determination in peptides. *J Magn Reson* 129(1):85–92.
- DiMaio F, Leaver-Fay A, Bradley P, Baker D, André I (2011) Modeling symmetric macromolecular structures in Rosetta3. *PLoS ONE* 6(6):e20450.
- Tsuboi M, Overman SA, Thomas GJ, Jr (1996) Orientation of tryptophan-26 in coat protein subunits of the filamentous virus Ff by polarized Raman microspectroscopy. *Biochemistry* 35(32):10403–10410.
- Marvin DA (1990) Model-building studies of Inovirus: Genetic variations on a geometric theme. *Int J Biol Macromol* 12(2):125–138.
- Tomar S (2006) Lyotropic liquid crystals of eight filamentous bacteriophages. PhD dissertation (Polytechnic University, Brooklyn, NY).
- Williams KA, et al. (1995) Packing of coat protein amphipathic and transmembrane helices in filamentous bacteriophage M13: Role of small residues in protein oligomerization. *J Mol Biol* 252(1):6–14.
- Roth TA, Weiss GA, Eigenbrot C, Sidhu SS (2002) A minimized M13 coat protein defines the requirements for assembly into the bacteriophage particle. *J Mol Biol* 322(2):357–367.
- Matsuno M, Takeuchi H, Overman SA, Thomas GJ, Jr (1998) Orientations of tyrosines 21 and 24 in coat subunits of Ff filamentous virus: Determination by Raman linear intensity difference spectroscopy and implications for subunit packing. *Biophys J* 74(6):3217–3225.
- Clack BA, Gray DM (1992) Flow linear dichroism spectra of four filamentous bacteriophages: DNA and coat protein contributions. *Biopolymers* 32(7):795–810.
- Takeuchi H, Matsuno M, Overman SA, Thomas GJ (1996) Raman linear intensity difference of flow-oriented macromolecules: Orientation of the indole ring of tryptophan-26 in filamentous virus fd. *J Am Chem Soc* 118(14):3498–3507.
- Takegoshi K, Nakamura S, Terao T (2001) C-13-H-1 dipolar-assisted rotational resonance in magic-angle spinning NMR. *Chem Phys Lett* 344(5-6):631–637.
- Morcombe CR, Gaponenko V, Byrd RA, Zilm KW (2004) Diluting abundant spins by isotope edited radio frequency field assisted diffusion. *J Am Chem Soc* 126(23):7196–7197.
- Hou G, Yan S, Trébois J, Amoureux J-P, Polenova T (2013) Broadband homonuclear correlation spectroscopy driven by combined R2(n)/v sequences under fast magic angle spinning for NMR structural analysis of organic and biological solids. *J Magn Reson* 232:18–30.
- Leaver-Fay A, et al. (2013) Scientific benchmarks for guiding macromolecular energy function improvement. *Methods Enzymol* 523:109–143.
- Shen Y, Vernon R, Baker D, Bax A (2009) De novo protein structure generation from incomplete chemical shift assignments. *J Biomol NMR* 43(2):63–78.
- Chen VB, et al. (2010) MolProbity: All-atom structure validation for macromolecular crystallography. *Acta Crystallogr D Biol Crystallogr* 66(Pt 1):12–21.
- Eisenberg D, Schwarz E, Komaromy M, Wall R (1984) Analysis of membrane and surface protein sequences with the hydrophobic moment plot. *J Mol Biol* 179(1):125–142.